Supplemental information

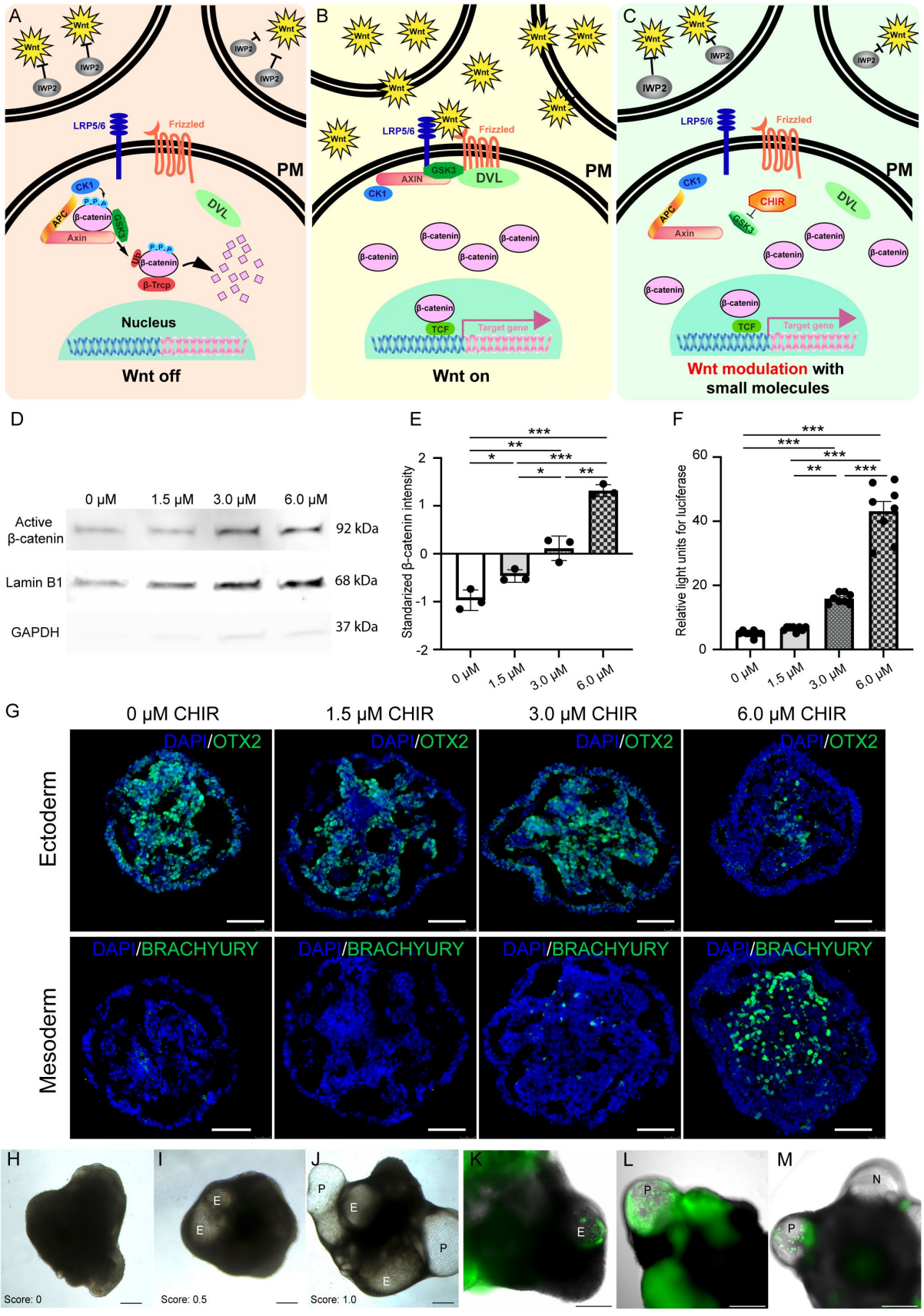
A
B
C
Wnt
IWP2
LRP5/6
Frizzled
PM
CK1
APC
β-catenin
Axin
GSK3
DVL
β-Trcp
Nucleus
Wnt off
AXIN
Target gene
TCF
Wnt on
CHIR
Wnt modulation with
small molecules
D
0 μM
1.5 μM
3.0 μM
6.0 μM
Active
β-catenin
92 kDa
Lamin B1
68 kDa
GAPDH
37 kDa
E
Standarized β-catenin intensity
F
Relative light units for luciferase
G
0 μM CHIR
1.5 μM CHIR
3.0 μM CHIR
6.0 μM CHIR
Ectoderm
Mesoderm
DAPI/OTX2
DAPI/BRACHYURY
H
I
J
K
L
M
Score: 0
Score: 0.5
Score: 1.0
E
P
N

Figure S1. Wnt modulation during the early induction of inner ear organoids. Related to figure 1. A-C. Schematic of the Wnt modulation process. A. Supplementation with the Wnt inhibitor IWP2 inhibits the secretion of Wnt ligands. B. When Wnt ligands bind to frizzle receptors, there is an intracellular increase in β-catenin. C. Supplementation with the Wnt activator CHIR99021 (CHIR) activates the canonical Wnt signaling pathway by inhibiting the degradation of β-catenin. D-E. Representative Western blot image (D) and data (E) showing a positive association between CHIR level and β-catenin concentrations. Lamin B was the reference (control) protein for the nuclear fraction. The lack of GAPDH signals indicates no contamination from the cytoplasmic fraction. Data in E were normalized to total nuclear protein (mean±SD). Each dot represents individual differentiation experiment. F. Aggregates were treated with various levels of Wnt activations and TCF/LEF-mediated luciferase activity was used to examine the responses to Wnt modulation. E & F. One-way ANOVA (p<0.001) followed by *post-hoc* tests: *p<0.05, **p<0.001, ***p<0.0001. G. Representative immunohistochemistry (IHC) images of the germ layer cells in aggregates of the three Wnt modulation treatments (day four). Ectodermal marker: OTX2. Mesodermal marker: Brachyury. H-J. Representative bright field (BF) images of aggregates. E: “embedded” otic vesicle (OV). P: protruding OV. Scores of 0, 0.5, and 1 were given when there were no visible OVs, when only embedded OVs were seen, and when protruding OVs were observed, respectively. L-M. Representative BF images of immature hair cells with *Atoh1*-2A-GFP fluorescent signals in OVs. E and P: as in the prior panel. N: OV without GFP signal. Scale bar=100 μm. (n=3-8 independent differentiation experiments)

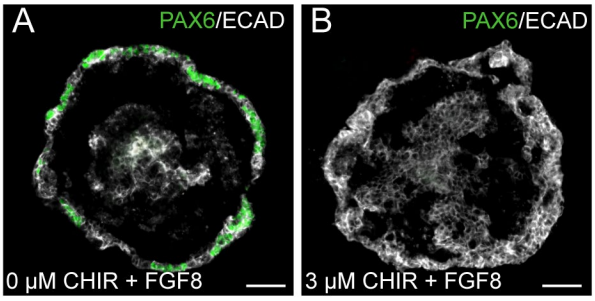

Figure S2. Expression of the anterior marker PAX6 in day-8 (D8) samples. Related to figure 2. Representative immunohistochemistry image of PAX6 and the epithelial marker E-cadherin (ECAD). A more pronounced PAX6 signal was seen in the outer layer of 0 µM CHIR samples when another FGF recombinant protein, FGF8, was added on D4 of induction. Scale bar=50 µm. (n=3 independent differentiation experiments)

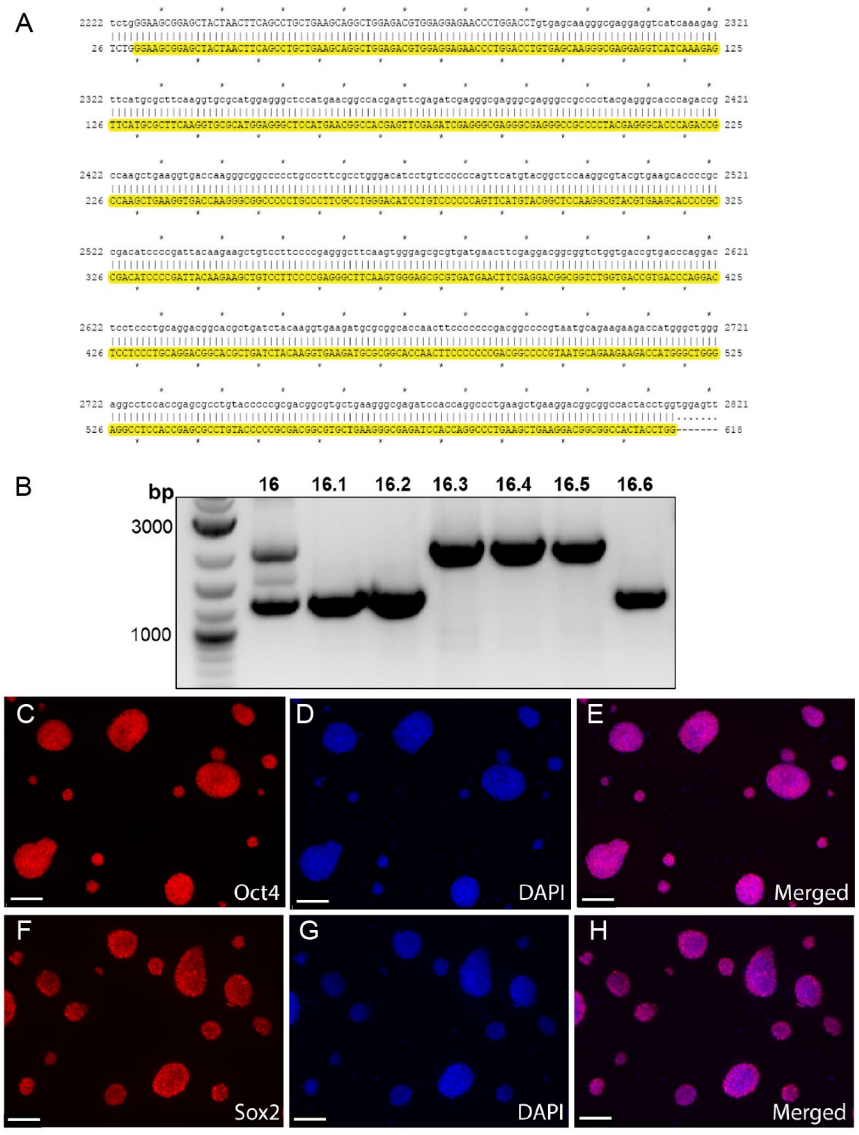

Figure S3. Validation of the *Pax8*-tdTomato reporter mouse embryonic stem cell (mESC) line. Related to figure 1-2. A. Sequence confirming successful insertion of the td-Tomato cassette (yellow) into the 3' end of the *Pax8* coding sequence. B. PCR results showing mESC colonies with homozygous tdTomato inserts (colonies 16.3-16.5). Colony 16.5 was used for all subsequent experiments. C-H. Representative immunohistochemistry images of two pluripotency markers: Oct4 and Sox2. Scale bar = 100 μm.

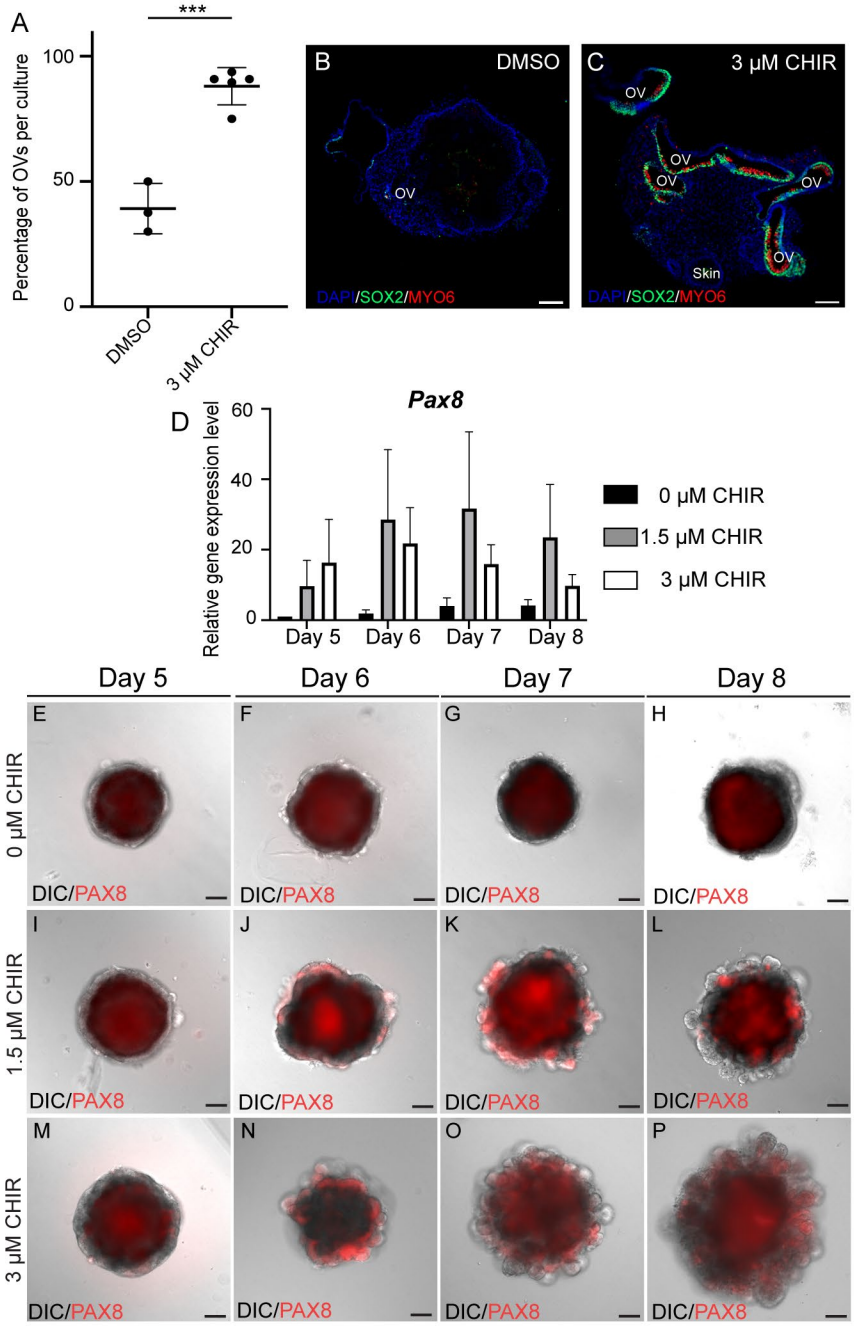

Figure S4. Wnt modulation increases generation of otic vesicles (OVs) in the Pax8-tdTomato reporter cell line. Related to figure 1-2. A. A higher percentage of OVs per differentiation experiment was documented in 3 μM CHIR samples than in the DMSO controls (*t*-test ****p*<0.0001). Representative IHC image of a D20 inner ear organoid of DMSO controls (B) and 3 μM CHIR group (C). D. Mean (±SD) gene expression levels of *Pax8* among various Wnt

levels. E-P. Representative BF images of *Pax8*-tdTomato signals across three Wnt levels during the early inner ear induction period. More prominent *Pax8*-tdTomato fluorescent signals were seen in the outer layers of 1.5 and 3 μM CHIR samples from D6 onwards. Scale bars=100 μm. n=3-5 independent differentiation experiments.

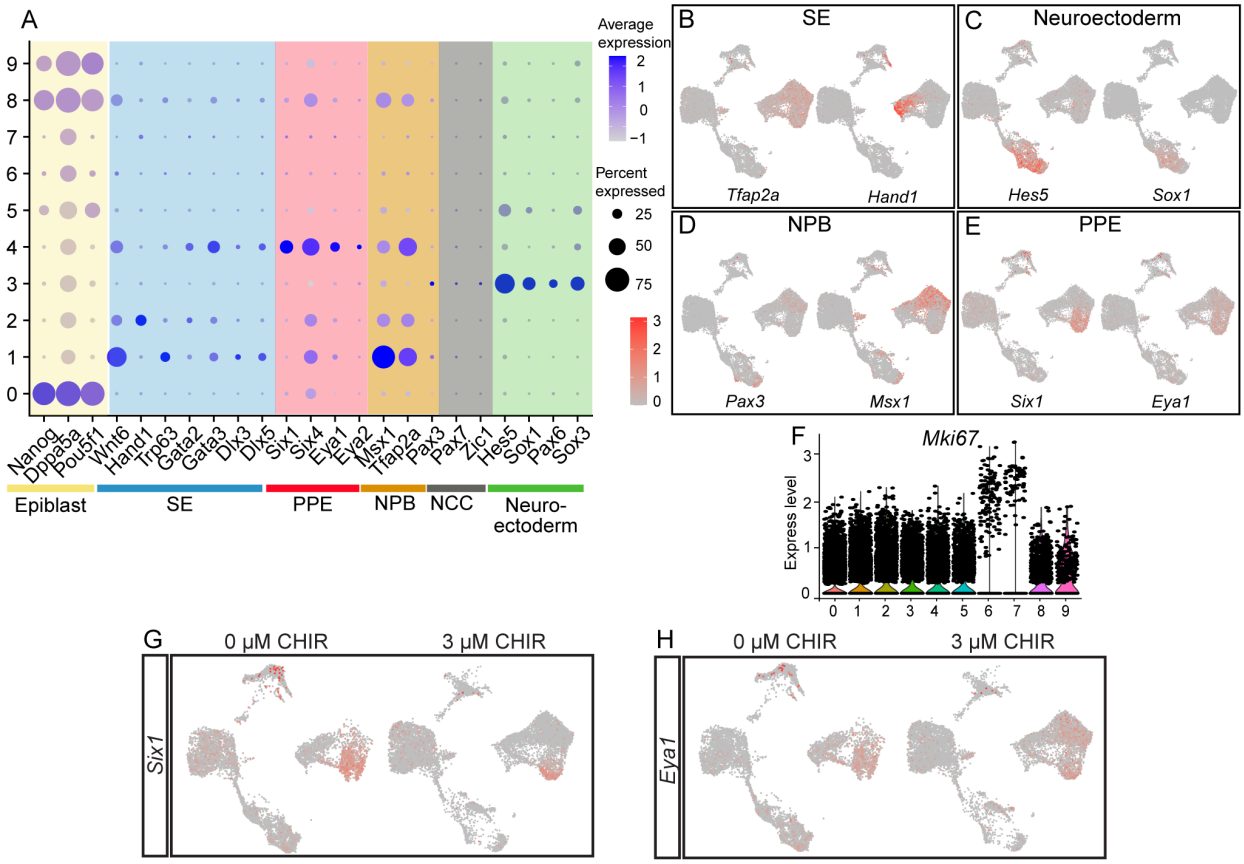

Figure S5. Single-cell RNA-sequencing (scRNA-seq) analyses on day-5 (D5) of the induction of inner ear organoids. Related to figure 4. A. Dot plot of cell lineage markers. B-E. Expression of lineage marker genes from the uniform manifold approximation and projection (UMAP). F. Violin plot of the cycling marker *Mki67* across induction days. G-H. Expression of two pre-placodal ectoderm (PPE) marker genes, *Six1* and *Eya1*, in the UMAP of the 0 and 3 μM CHIR treatments. More *Six1*$^{+}$ PPE cells were seen in 0 μM CHIR samples on D5.

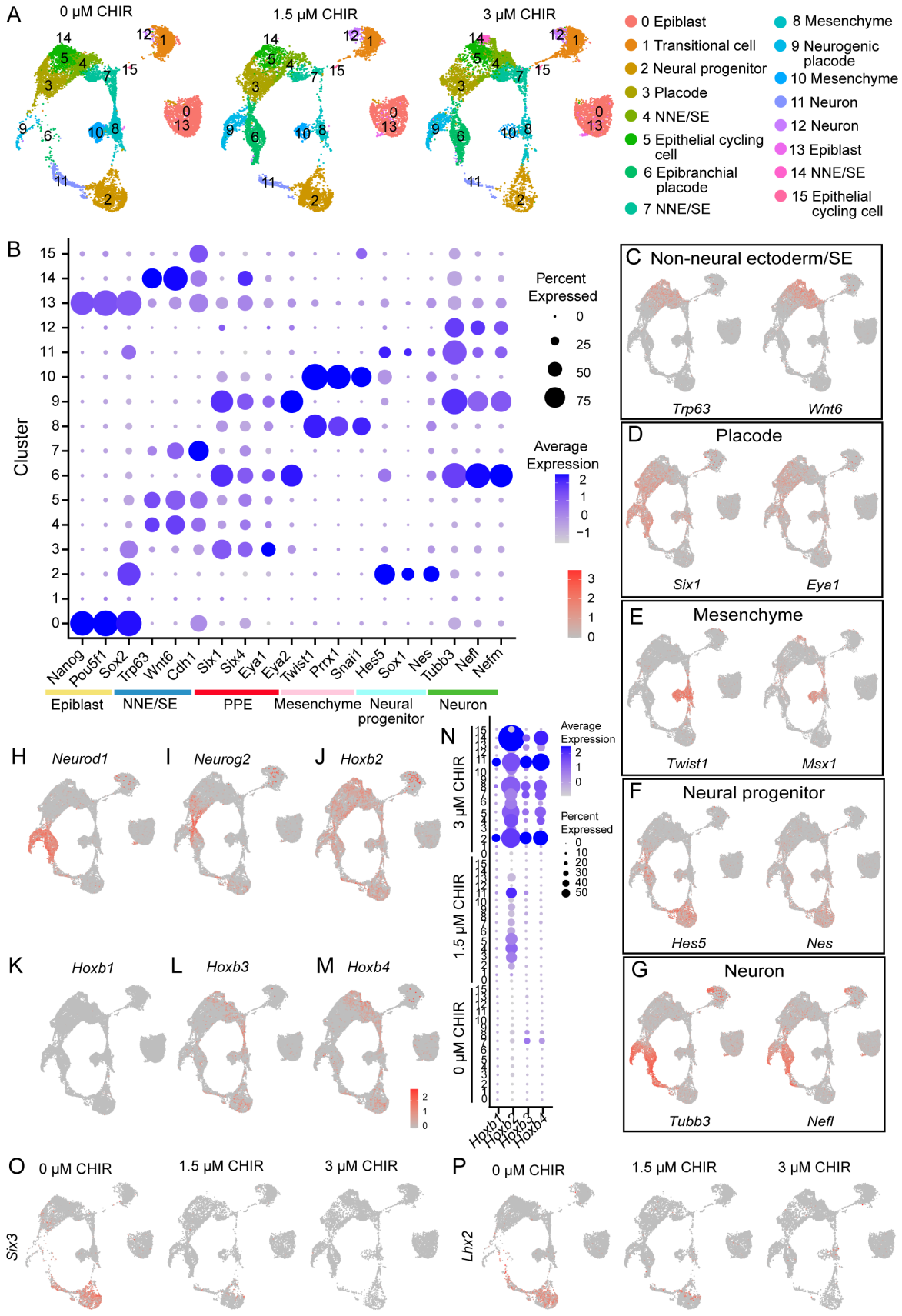
A
0 μM CHIR
1.5 μM CHIR
3 μM CHIR
0 Epiblast
1 Transitional cell
2 Neural progenitor
3 Placode
4 NNE/SE
5 Epithelial cycling cell
6 Epibranchial placode
7 NNE/SE
8 Mesenchyme
9 Neurogenic placode
10 Mesenchyme
11 Neuron
12 Neuron
13 Epiblast
14 NNE/SE
15 Epithelial cycling cell
B
Cluster
Percent Expressed
Average Expression
Nanog
Pou5f1
Sox2
Trp63
Wnt6
Cdh1
Six1
Six4
Eya1
Eya2
Twist1
Prrx1
Snai1
Hes5
Sox1
Nes
Tubb3
Nefl
Neifm
Epiblast
NNE/SE
PPE
Mesenchyme
Neural progenitor
Neuron
C Non-neural ectoderm/SE
Trp63
Wnt6
D Placode
Six1
Eya1
E Mesenchyme
Twist1
Msx1
F Neural progenitor
Hes5
Nes
G Neuron
Tubb3
Nefl
H Neurod1
I Neurog2
J Hoxb2
K Hoxb1
L Hoxb3
M Hoxb4
N
3 μM CHIR
1.5 μM CHIR
0 μM CHIR
Hoxb1
Hoxb2
Hoxb3
Hoxb4
O 0 μM CHIR
1.5 μM CHIR
3 μM CHIR
Six3
P 0 μM CHIR
1.5 μM CHIR
3 μM CHIR
Lhx2

Figure S6. scRNA-seq analyses of samples of each of the three Wnt treatment groups during inner ear organoid induction (day-8 [D8]). Related to figure 5. A. Uniform manifold approximation and projection (UMAP) of D8 samples of the 0, 1.5, and 3 μM CHIR treatments; 15 clusters were manually annotated based on lineage markers. NNE: non-neural ectoderm. SE: surface ectoderm. B. Dot plot of lineage markers. C-G. Feature plots of selected lineage markers. H. The neural placodal marker *Neurod1* was seen in placodal clusters 6 and 9. I. Expression of *Neurog2* in the presumably epibranchial placode cluster (#9). J. Feature plot of *Hoxb2*, which was found in the largest number of cells. K-M. Feature plots of anterior *Hox* genes. N. Dot plot of expression trends of anterior *Hox* genes among clusters of the 0, 1.5, and 3 μM CHIR treatments. O-P. Feature plots of two forebrain markers in samples of the three Wnt treatments. Forebrain marker gene expression levels decreased as the Wnt activation level increased.

Table S1. Marker gene list

Cell type	Gene	Citations
Pluripotency/Epiblast	Nanog	(Baker, 2009; Mitsui et al., 2003; Silva et al., 2009)
Pluripotency/Epiblast	Dppa5a	(Kim et al., 2005; Morgani et al., 2017)
Pluripotency/Epiblast	Pou5f1	(Masui et al., 2007; Okamoto et al., 1990)
Pluripotency/Epiblast	Sox2	(Adachi et al., 2010; Avilion et al., 2003; Masui et al., 2007)
Non-neuroectoderm/ Surface ectoderm	Wnt6	(Geetha-Loganathan et al., 2006; Lee et al., 2020; Tchieu et al., 2017)
Non-neuroectoderm/ Surface ectoderm	Trp63	(Koster and Roop, 2007; Soares and Zhou, 2018; Tchieu et al., 2017)
Non-neuroectoderm/ Surface ectoderm	Hand1	(Lee et al., 2020; Mokry and Pisal, 2020)
Non-neuroectoderm/ Surface ectoderm	Gata2	(Sheng and Stern, 1999; Streit, 2007; Thawani and Groves, 2020)
Non-neuroectoderm/ Surface ectoderm	Gata3	(Qu et al., 2016; Sheng and Stern, 1999; Streit, 2007)
Non-neuroectoderm/ Surface ectoderm	Dlx3	(Feledy et al., 1999; Luo et al., 2001; Pieper et al., 2012)

Non-neuroectoderm/ Surface ectoderm	Dlx5	(Luo et al., 2001; Pieper et al., 2012; Streit, 2007)
Non-neuroectoderm/ Surface ectoderm	Cdh1	(Nikolopoulou et al., 2019; Qu et al., 2016)
Non-neuroectoderm/ Surface ectoderm	Krt8	(Aberdam et al., 2007; Kogut and Bilousova, 2019; Qu et al., 2016)
Non-neuroectoderm/ Surface ectoderm	Krt18	(Aberdam et al., 2007; Kogut and Bilousova, 2019; Qu et al., 2016)
PPE	Six1	(Christophorou et al., 2009; Litsiou et al., 2005; Thawani and Groves, 2020)
PPE	Six4	(Christophorou et al., 2009; Litsiou et al., 2005; Thawani and Groves, 2020)
PPE	Eya1	(Christophorou et al., 2009; Streit, 2007; Thawani and Groves, 2020)
PPE	Eya2	(Christophorou et al., 2009; Streit, 2007; Thawani and Groves, 2020)
NPB	Msx1	(Pla and Monsoro-Burq, 2018; Roellig et al., 2017; Thawani and Groves, 2020)
NPB	Tfap2a	(de Crozé et al., 2011; Roellig et al., 2017; Rothstein and Simoes-Costa, 2020)

NPB	Pax3	(de Crozé et al., 2011; Milet and Monsoro-Burq, 2012; Thier et al., 2019)
Neuroectoderm/neural progenitor	Hes5	(Edri et al., 2015; Ohtsuka et al., 2001)
Neuroectoderm/neural progenitor	Sox1	(Edri et al., 2015; Venere et al., 2012)
Neuroectoderm/neural progenitor	Pax6	(Edri et al., 2015; Tchieu et al., 2017)
Neuroectoderm/neural progenitor	Sox3	(Streit, 2007; Venere et al., 2012)
Neuroectoderm/neural progenitor	Nestin	(Bernal and Arranz, 2018; Hendrickson et al., 2011)
Neuron	Tubb3	(Latremoliere et al., 2018; Wright et al., 2021)
Neuron	Nefl	(Kim et al., 2021; Smits et al., 2020)
Neuron	Nefm	(Kim et al., 2021; Smits et al., 2020)
Mesenchyme	Twist1	(Bildsoe et al., 2016; Chen and Behringer, 1995; Soldatov et al., 2019)
Mesenchyme	Prrx1	(Fazilaty et al., 2019; Guo et al., 2015; ten Berge et al., 2001)

Mesenchyme	Prrx2	(Carr et al., 2019; Higuchi et al., 2015; ten Berge et al., 2001)
Mesenchyme	Snail1	(Batlle et al., 2013; Fazilaty et al., 2019; Rowe et al., 2009)

Table S2. Primer list.

Gene	Host
Otx2	forward: GCTCTGTTTGCCAAGACCCG
	reverse: ACCATACCTGCACCCTGGAT
Gbx2	forward: GGATGCGGAAGACGGCAAAG
	reverse: CGGACAGCCCCGACGAG
Pax 6	forward: TGGTGTCTTTGTCAACGGGC
	reverse: TTTTGCATCTGCATGGGTCTGC
Pax8	forward: AATCATCCGGACCAAAGTGCAGC
	reverse: CTGAGCTGGGGATCAGTGTGTGT
L27	forward: CGTCATCGTGAAGAACATTG
	reverse: CATGGCAGCTGTCACTTTC

Table S3. Antibody list. IHC=immunohistochemistry**.** W=western blot.

Primary antibodies	**Host**	**Supplier**	**Cat. no**	**Application**	**Dilution**
Brachyury	Goat	R&D	AF2085	IHC	1:20
Active β-catenin	Rabbit	Millepore	05-665	W	1:1000
E-Cadherin	Mouse	BD Biosciences	610181	IHC	1:50
EYA1	Rabbit	Proteintech	22658-1-AP	IHC	1:100
FBXO2	Rabbit	Proteintech	14590-1-AP	IHC	1:50
GAPDH	Rabbit	CST	5174	W	1:1000
GBX2	Goat	Abcam	Ab109726	IHC	1:125
Lamin B1	Rabbit	CST	13435	W	1:500
MSX1	Mouse	DSHB	4G1	IHC	1:5
Myosin-VI	Rabbit	Proteus	25-6791	IHC	1:100
Myosin-VIIA	Rabbit	Proteus	25-6790	IHC	1:100
Oct-3/4 (C-10)	Mouse	Santa Cruz	sc-5279	IHC	1:100
OTX2	Goat	R&D	AF1979	IHC	1:20
PAX6	Mouse	DSHB	Pax6	IHC	1:5
PAX8	Rabbit	Abcam	ab97477	IHC	1:100

SIX1	Rabbit	Sigma-Aldrich	HPA001893	IHC	1:250
SOX2	Mouse	BD Biosciences	561469	IHC	1:50
SOX10	Rabbit	Abcam	Ab155279	IHC	1:50

Supplemental experimental procedures.

mESC culture and induction of inner ear organoids. The LIF-2i media contained a 1:1 ratio of Advanced DMEM-F12 (Gibco) and Neurobasal medium (Gibco), 1X N2 supplement (Thermo-Fisher Scientific [TFS]), 1X B-27 supplement without vitamin A (TFS), 1X Glutamax (Gibco), 1X normocin (Invivogen), 1000 unit of Lif (Millepore), 3 μM CHIR99021 (Stemcell Technologies), and 1.5 μM CGP77675 (Sigma).

Briefly, ESCs were dissociated in Accutase (Stemcell Technologies) and re-suspended in differentiation media (DMLK). On D0, 1,500 or 3,000 cells (depending on cell lines) in 100 μl DMLK per well were plated in low-binding, 96-well U-bottom plates (TFS). Half of the media was exchanged with fresh DMLK containing Matrigel (Corning; 2% final concentration) on D1. BMP4 (PromoKine), SB-431542 (Reprocell), 4 μM IWP2 (Stemcell Technologies), and various concentrations of CHIR99021 were added on D2 or D3 depending on cell lines. After 24 hr, FGF2 (Stemcell Technologies) and LDN-193189 (Reprocell) were added. On D8, aggregates were washed twice in Advanced DMEM/F12 before transfer to a new, 96-well U-bottom plate with 100 μl N2 media (containing Advanced DMEM/F12, 1X N2, 1X Glutamax, & 1X normocin) containing 1% Matrigel and 3 μM CHIR99021 (optional). After 48 hr, aggregates were transferred to 24-well low-binding plates with fresh N2 media until D20. Half of the media was changed every other day during this long-term culture period.

OV productivity Embedded OVs were scored as 0.5, and protruding OVs were scored as 1 (Figure S1G-I). Scores of 0 were given to aggregates without any visible OVs. The percentage of OVs per culture was calculated as the total score divided by the total number of aggregates in one culture. Each independent culture therefore served as one biological replicate. The percentage of hair cell-bearing OVs was conducted using the *Atoh1*-2A-nGFP reporter cell line.

The numbers of GFP^+ OVs and total vesicles were counted in each culture (Figure S1 J-L), and the percentages of hair cell-bearing OVs were reported as GFP^+ OVs/total vesicles x 100.

Cloning of Pax8 sgRNA and Cas9 co-expression construct and donor plasmid repair template A Pax8 guide RNA was inserted into the pSpCas9(BB)-2A-Puro (pX459) vector (Ran et al., 2013) (Addgene plasmid #48139) as follows. Briefly, the pX459 vector was digested with BbsI (NEB) and treated with T4 PNK (NEB); the linearized vector was then gel purified. A pair of oligos for the Pax8 target site (sense: CACCGTGACAACTACAGATGGTCAA; antisense: AAACTTGACCATCTGTAGTTGTCAC) was annealed, phosphorylated, and ligated to the linearized PX459 vector. Next, we cloned a plasmid-based (pcDNA3.1) donor repair template that contained 1-kb homology arms flanking a p2A-tdTomato coding sequence. The two homology arms were designed around the Pax8-targeting site. Both the SpCas9 plasmid containing the Pax8 sgRNA and the donor plasmid repair template were verified by sequencing.

Co-transfection of Cas9-Pax8, the sgRNA plasmid, and a homology-directed repair (HDR) template for the Pax8-tdTomato cell line We seeded 5 x 10^4 cells/well on a 24-well plate for transfection. The following day, we co-transfected 500 ng of SpCas9 plasmid containing Pax8 sgRNA along with 1 μg of linearized donor repair template into cells using Lipofectamine 3000 Reagent (TFS). At 48 hr post-transfection, cells were dissociated with Accutase (Corning) and resuspended gently in a 5X volume of stem cell media; 50 ml of this media included 24 ml Advanced DMEM/F12, 24 ml Neurobasal media, 250 µl N2 supplement, 500 µl B-27 supplement (TFS), 500 µl glutamine (TFS), 50 µl 2-mercaptoethanol (TFS), and 500 µl penicillin-streptomycin (TFS) after which the following were added freshly to create a single-cell suspension: 1 μM PD0325901 (Reprocell), 3 uM CHIR99021, and 1000 units/ml Lif. The cells were seeded on a 60-mm dish to form single cell colonies. The next day, puromycin selection was initiated to select transfected cells by replacing the media with fresh media containing 0.5 μg/ml puromycin (TFS). The selection process continued for five days in puromycin-containing

media after which the media was changed to regular media. The media was changed every 2-3 days once the colonies began to form and proliferate. Once the colonies were large enough to be picked, they were carefully marked for picking and transferred into 96-well plates (one well/colony). Once the stem cell colonies reached 60% confluency, they were passaged to prepare replicate plates. The colonies were dissociated by treating them briefly with Accutase and pipetting up and down vigorously by adding 100 µl media directly into the wells. We plated 20% of each of the resuspended volumes into the replicate wells to keep the clonal lines growing, using the remaining 80% of the cells for DNA isolation and genotyping.

Validation of the Pax8-tdTomato cell line We analyzed all colonies for presence of the tdTomato knock-in sequence by performing a simple PCR-based screening technique. For this, we designed a pair of PCR primers both upstream and downstream of the left and right homology arms (used to create the repair donor template), respectively, of the *Pax8* genomic loci: *Pax8* genomic F (CAGCTCTACATCAAGGCCAAG) and *Pax8* genomic R (GGAAAGTGAATGACTGGCATG). This primer pair yielded a 1,278-bp fragment from the wild type allele and a 2,769-bp fragment from the *Pax8*-td tomato knock-in allele. We performed this PCR screen for all clones, and the knock-in colonies were selected for further experimentation.

Western blots SDS-PAGE was conducted using 4-20% TGX stain-free mini gels (Bio-Rad). Stain-free gels prior to transfer were imaged as total protein references using the ChemiDoc Touch Imaging System (Bio-Rad). The transfer was conducted using the Trans-Blot®Turbo™ transfer system (Bio-Rad) under the program “1 TGX-mini gel.” The blot was blocked in 5% non-fat milk (Rockland) in TBST (0.005% Tween 20 [Sigma] in 1X TBS [Bio-Rad]) at RT for 1 hr followed by incubation in the primary antibody solution (Table S3) at 4°C overnight on the shaker. The next day, the blot was washed thrice with TBST for 5 min followed by a 1-hr incubation in the secondary antibody solution with HRP-conjugated secondary antibody (Bio-Rad) at RT. The blot was then washed thrice in TBST for 5 min before signal development using

Clarity ECL Western Substrates (Bio-Rad). Imaging was acquired using the ChemiDoc Touch Imaging System.

scRNA-seq of inner ear organoids Approximately 12-48 organoids (depending on culture day) were dissociated in TrypLE Express (TFS) at 37˚C with shaking for 30-45 min. During dissociation, samples were mixed via pipetting every 5-10 min. Dissociated cells were filtered through a 40-μM cell strainer (Flowmi) followed by three washes with DPBS+2% BSA. Single cell 3' RNA-seq experiments were conducted using the Chromium single cell system (10X Genomics) and Illumina sequencers at the Center for Medical Genetics (CMG) of the Indiana University School of Medicine. Each cell suspension was first inspected on the Countess II FL (TFS) and under a microscope for assessment of cell number, viability, and size. Depending on the quality of the initial cell suspension, the single-cell preparation included centrifugation, re-suspension, and filtration to remove cell debris, dead cells, and cell aggregates. Single-cell capture and library preparation were carried out according to the Chromium Single Cell 3' reagent kits (V3) user guide (10X Genomics). The appropriate number of cells were loaded on a multiple-channel micro-fluidics chip of the Chromium Single Cell Instrument (10X Genomics) with a targeted cell recovery of 10,000. Single-cell gel beads in emulsion containing barcoded oligonucleotides and reverse transcriptase reagents were generated with the single-cell reagent kit (V3; 10X Genomics). Following cell capture and lysis, cDNA was synthesized and amplified. Illumina sequencing libraries were then prepared with the amplified cDNA. The resulting libraries were assessed with an Agilent TapeStation or Bioanalyzer 2100. The final libraries were sequenced using a custom program on an Illumina NovaSeq 6000, which generated a 26-bp cell barcode followed by a UMI barcode followed by the 91-bp RNA read.

scRNA-seq data analyses We normalized and scaled the matrix using Seurat's NormalizeData and ScaleData functions, respectively, and defined the top 2,000 highly variable genes for each sample using Seurat's FindVariableFeatures function. To integrate multiple samples across different days and conditions, we used Seurat's FindIntegrationAnchors function to find the

anchors and integrate all samples using the IntegrateData function based on the identified anchors. The highly variable genes were used for principal components analysis via Seurat's RunPCA function. The first 30 principal components were used for UMAP visualization and Louvain clustering using the RunUMAP and FindClusters functions, respectively. Annotation of clusters was done manually based on the expression of marker genes (Table S1). We then used Seurat's FindConservedMarkers function to identify the canonical cell type-specific gene markers conserved between sample groups, and the FindMarkers function was used to identify cell type-specific DEGs between treatments on each day.

References

Aberdam, D., Gambaro, K., Medawar, A., Aberdam, É., Rostagno, P., de la Forest Divonne, S., and Rouleau, M. (2007). Embryonic stem cells as a cellular model for neuroectodermal commitment and skin formation. Comptes Rendus Biologies *330*, 479-484.

Adachi, K., Suemori, H., Yasuda, S.-y., Nakatsuji, N., and Kawase, E. (2010). Role of SOX2 in maintaining pluripotency of human embryonic stem cells. Genes to Cells *15*, 455-470.

Avilion, A.A., Nicolis, S.K., Pevny, L.H., Perez, L., Vivian, N., and Lovell-Badge, R. (2003). Multipotent cell lineages in early mouse development depend on SOX2 function. Genes Dev *17*, 126-140.

Baker, M. (2009). What does Nanog do? Nature Reports Stem Cells.

Batlle, R., Alba-Castellón, L., Loubat-Casanovas, J., Armenteros, E., Francí, C., Stanisavljevic, J., Banderas, R., Martin-Caballero, J., Bonilla, F., Baulida, J.*, et al.* (2013). Snail1 controls TGF-β responsiveness and differentiation of mesenchymal stem cells. Oncogene *32*, 3381-3389.

Bernal, A., and Arranz, L. (2018). Nestin-expressing progenitor cells: function, identity and therapeutic implications. Cellular and Molecular Life Sciences *75*, 2177-2195.

Bildsoe, H., Fan, X., Wilkie, E.E., Ashoti, A., Jones, V.J., Power, M., Qin, J., Wang, J., Tam, P.P.L., and Loebel, D.A.F. (2016). Transcriptional targets of TWIST1 in the cranial mesoderm regulate cell-matrix interactions and mesenchyme maintenance. Dev Biol *418*, 189-203.

Carr, M.J., Toma, J.S., Johnston, A.P.W., Steadman, P.E., Yuzwa, S.A., Mahmud, N., Frankland, P.W., Kaplan, D.R., and Miller, F.D. (2019). Mesenchymal Precursor Cells in Adult Nerves Contribute to Mammalian Tissue Repair and Regeneration. Cell Stem Cell *24*, 240-256.e249.

Chen, Z.F., and Behringer, R.R. (1995). twist is required in head mesenchyme for cranial neural tube morphogenesis. Genes Dev *9*, 686-699.

Christophorou, N.A.D., Bailey, A.P., Hanson, S., and Streit, A. (2009). Activation of Six1 target genes is required for sensory placode formation. Developmental Biology *336*, 327-336.

de Crozé, N., Maczkowiak, F., and Monsoro-Burq, A.H. (2011). Reiterative AP2a activity controls sequential steps in the neural crest gene regulatory network. Proceedings of the National Academy of Sciences *108*, 155-160.

Edri, R., Yaffe, Y., Ziller, M.J., Mutukula, N., Volkman, R., David, E., Jacob-Hirsch, J., Malcov, H., Levy, C., Rechavi, G*., et al.* (2015). Analysing human neural stem cell ontogeny by consecutive isolation of Notch active neural progenitors. Nature Communications *6*, 6500.

Fazilaty, H., Rago, L., Kass Youssef, K., Ocaña, O.H., Garcia-Asencio, F., Arcas, A., Galceran, J., and Nieto, M.A. (2019). A gene regulatory network to control EMT programs in development and disease. Nature Communications *10*, 5115.

Feledy, J.A., Beanan, M.J., Sandoval, J.J., Goodrich, J.S., Lim, J.H., Matsuo-Takasaki, M., Sato, S.M., and Sargent, T.D. (1999). Inhibitory Patterning of the Anterior Neural Plate in Xenopus by Homeodomain Factors Dlx3 and Msx1. Developmental Biology *212*, 455-464.

Geetha-Loganathan, P., Nimmagadda, S., Huang, R., Christ, B., and Scaal, M. (2006). Regulation of ectodermal Wnt6 expression by the neural tube is transduced by dermomyotomal Wnt11: a mechanism of dermomyotomal lip sustainment. Development *133*, 2897-2904.

Guo, J., Fu, Z., Wei, J., Lu, W., Feng, J., and Zhang, S. (2015). PRRX1 promotes epithelial-mesenchymal transition through the Wnt/β-catenin pathway in gastric cancer. Med Oncol *32*, 393.

Hendrickson, M.L., Rao, A.J., Demerdash, O.N.A., and Kalil, R.E. (2011). Expression of Nestin by Neural Cells in the Adult Rat and Human Brain. PLOS ONE *6*, e18535.

Higuchi, M., Kato, T., Yoshida, S., Ueharu, H., Nishimura, N., and Kato, Y. (2015). PRRX1- and PRRX2-positive mesenchymal stem/progenitor cells are involved in vasculogenesis during rat embryonic pituitary development. Cell Tissue Res *361*, 557-565.

Kim, D.W., Liu, K., Wang, Z.Q., Zhang, Y.S., Bathini, A., Brown, M.P., Lin, S.H., Washington, P.W., Sun, C., Lindtner, S.*, et al.* (2021). Gene regulatory networks controlling differentiation, survival, and diversification of hypothalamic Lhx6-expressing GABAergic neurons. Communications Biology *4*, 95.

Kim, S.-K., Suh, M.R., Yoon, H.S., Lee, J.B., Oh, S.K., Moon, S.Y., Moon, S.-H., Lee, J.Y., Hwang, J.H., Cho, W.J.*, et al.* (2005). Identification of Developmental Pluripotency Associated 5 Expression in Human Pluripotent Stem Cells. STEM CELLS *23*, 458-462.

Kogut, I., and Bilousova, G. (2019). Environmental Influences on the Development of Epidermal Progenitors. In Encyclopedia of Tissue Engineering and Regenerative Medicine, R.L. Reis, ed. (Oxford: Academic Press), pp. 243-254.

Koster, M.I., and Roop, D.R. (2007). Mechanisms regulating epithelial stratification. Annu Rev Cell Dev Biol *23*, 93-113.

Latremoliere, A., Cheng, L., DeLisle, M., Wu, C., Chew, S., Hutchinson, E.B., Sheridan, A., Alexandre, C., Latremoliere, F., Sheu, S.-H.*, et al.* (2018). Neuronal-Specific TUBB3 Is Not Required for Normal Neuronal Function but Is Essential for Timely Axon Regeneration. Cell Rep *24*, 1865-1879.e1869.

Lee, J., Rabbani, C.C., Gao, H., Steinhart, M.R., Woodruff, B.M., Pflum, Z.E., Kim, A., Heller, S., Liu, Y., Shipchandler, T.Z.*, et al.* (2020). Hair-bearing human skin generated entirely from pluripotent stem cells. Nature *582*, 399-404.

Litsiou, A., Hanson, S., and Streit, A. (2005). A balance of FGF, BMP and WNT signalling positions the future placode territory in the head. Development *132*, 4051-4062.

Luo, T., Matsuo-Takasaki, M., and Sargent, T.D. (2001). Distinct roles for distal-less genes Dlx3 and Dlx5 in regulating ectodermal development in Xenopus. Molecular Reproduction and Development *60*, 331-337.

Masui, S., Nakatake, Y., Toyooka, Y., Shimosato, D., Yagi, R., Takahashi, K., Okochi, H., Okuda, A., Matoba, R., Sharov, A.A.*, et al.* (2007). Pluripotency governed by Sox2 via regulation of Oct3/4 expression in mouse embryonic stem cells. Nature Cell Biology *9*, 625-635.

Milet, C., and Monsoro-Burq, A.H. (2012). Neural crest induction at the neural plate border in vertebrates. Developmental Biology *366*, 22-33.

Mitsui, K., Tokuzawa, Y., Itoh, H., Segawa, K., Murakami, M., Takahashi, K., Maruyama, M., Maeda, M., and Yamanaka, S. (2003). The Homeoprotein Nanog Is Required for Maintenance of Pluripotency in Mouse Epiblast and ES Cells. Cell *113*, 631-642.

Mokry, J., and Pisal, R. (2020). Development and Maintenance of Epidermal Stem Cells in Skin Adnexa. International Journal of Molecular Sciences *21*, 9736.

Morgani, S., Nichols, J., and Hadjantonakis, A.-K. (2017). The many faces of Pluripotency: in vitro adaptations of a continuum of in vivo states. BMC Developmental Biology *17*, 7.

Nikolopoulou, E., Hirst, C.S., Galea, G., Venturini, C., Moulding, D., Marshall, A.R., Rolo, A., De Castro, S.C.P., Copp, A.J., and Greene, N.D.E. (2019). Spinal neural tube closure depends on regulation of surface ectoderm identity and biomechanics by Grhl2. Nature Communications *10*, 2487.

Ohtsuka, T., Sakamoto, M., Guillemot, F., and Kageyama, R. (2001). Roles of the Basic Helix-Loop-Helix Genes Hes1 and Hes5 in Expansion of Neural Stem Cells of the Developing Brain *. Journal of Biological Chemistry *276*, 30467-30474.

Okamoto, K., Okazawa, H., Okuda, A., Sakai, M., Muramatsu, M., and Hamada, H. (1990). A novel octamer binding transcription factor is differentially expressed in mouse embryonic cells. Cell *60*, 461-472.

Pieper, M., Ahrens, K., Rink, E., Peter, A., and Schlosser, G. (2012). Differential distribution of competence for panplacodal and neural crest induction to non-neural and neural ectoderm. Development *139*, 1175-1187.

Pla, P., and Monsoro-Burq, A.H. (2018). The neural border: Induction, specification and maturation of the territory that generates neural crest cells. Developmental Biology *444*, S36-S46.

Qu, Y., Zhou, B., Yang, W., Han, B., Yu-Rice, Y., Gao, B., Johnson, J., Svendsen, C.N., Freeman, M.R., Giuliano, A.E.*, et al.* (2016). Transcriptome and proteome characterization of surface ectoderm cells differentiated from human iPSCs. Scientific Reports *6*, 32007.

Roellig, D., Tan-Cabugao, J., Esaian, S., and Bronner, M.E. (2017). Dynamic transcriptional signature and cell fate analysis reveals plasticity of individual neural plate border cells. eLife *6*, e21620.

Rothstein, M., and Simoes-Costa, M. (2020). Heterodimerization of TFAP2 pioneer factors drives epigenomic remodeling during neural crest specification. Genome Res *30*, 35-48.

Rowe, R.G., Li, X.-Y., Hu, Y., Saunders, T.L., Virtanen, I., de Herreros, A.G., Becker, K.-F., Ingvarsen, S., Engelholm, L.H., Bommer, G.T.*, et al.* (2009). Mesenchymal cells reactivate Snail1 expression to drive three-dimensional invasion programs. Journal of Cell Biology *184*, 399-408.

Sheng, G., and Stern, C.D. (1999). Gata2 and Gata3: novel markers for early embryonic polarity and for non-neural ectoderm in the chick embryo. Mech Dev *87*, 213-216.

Silva, J., Nichols, J., Theunissen, T.W., Guo, G., van Oosten, A.L., Barrandon, O., Wray, J., Yamanaka, S., Chambers, I., and Smith, A. (2009). Nanog Is the Gateway to the Pluripotent Ground State. Cell *138*, 722-737.

Smits, L.M., Magni, S., Kinugawa, K., Grzyb, K., Luginbühl, J., Sabate-Soler, S., Bolognin, S., Shin, J.W., Mori, E., Skupin, A.*, et al.* (2020). Single-cell transcriptomics reveals multiple neuronal cell types in human midbrain-specific organoids. Cell and Tissue Research *382*, 463-476.

Soares, E., and Zhou, H. (2018). Master regulatory role of p63 in epidermal development and disease. Cellular and Molecular Life Sciences *75*, 1179-1190.

Soldatov, R., Kaucka, M., Kastriti, M.E., Petersen, J., Chontorotzea, T., Englmaier, L., Akkuratova, N., Yang, Y., Häring, M., Dyachuk, V.*, et al.* (2019). Spatiotemporal structure of cell fate decisions in murine neural crest. Science *364*.

Streit, A. (2007). The preplacodal region: an ectodermal domain with multipotential progenitors that contribute to sense organs and cranial sensory ganglia. Int J Dev Biol *51*, 447-461.

Tchieu, J., Zimmer, B., Fattahi, F., Amin, S., Zeltner, N., Chen, S., and Studer, L. (2017). A Modular Platform for Differentiation of Human PSCs into All Major Ectodermal Lineages. Cell Stem Cell *21*, 399-410.e397.

ten Berge, D., Brouwer, A., Korving, J., Reijnen, M.J., van Raaij, E.J., Verbeek, F., Gaffield, W., and Meijlink, F. (2001). Prx1 and Prx2 are upstream regulators of sonic hedgehog and control cell proliferation during mandibular arch morphogenesis. Development *128*, 2929-2938.

Thawani, A., and Groves, A.K. (2020). Building the Border: Development of the Chordate Neural Plate Border Region and Its Derivatives. Frontiers in Physiology *11*.

Thier, M.C., Hommerding, O., Panten, J., Pinna, R., García-González, D., Berger, T., Wörsdörfer, P., Assenov, Y., Scognamiglio, R., Przybylla, A.*, et al.* (2019). Identification of Embryonic Neural Plate Border Stem Cells and Their Generation by Direct Reprogramming from Adult Human Blood Cells. Cell Stem Cell *24*, 166-182.e113.

Venere, M., Han, Y.-G., Bell, R., Song, J.S., Alvarez-Buylla, A., and Blelloch, R. (2012). Sox1 marks an activated neural stem/progenitor cell in the hippocampus. Development *139*, 3938-3949.

Wright, C.M., Schneider, S., Smith-Edwards, K.M., Mafra, F., Leembruggen, A.J.L., Gonzalez, M.V., Kothakapa, D.R., Anderson, J.B., Maguire, B.A., Gao, T.*, et al.* (2021). scRNA-Seq Reveals New Enteric Nervous System Roles for GDNF, NRTN, and TBX3. Cellular and Molecular Gastroenterology and Hepatology *11*, 1548-1592.e1541.

Ran, F.A., Hsu, P.D., Wright, J., Agarwala, V., Scott, D.A., and Zhang, F. (2013). Genome engineering using the CRISPR-Cas9 system. Nat Protoc 8, 2281-2308.